AIP | The Journal of Chemical Physics

Regular and irregular vibrational states: Localized anharmonic modes in Ar 3

Nicholas J. Wright and Jeremy M. Hutson

Citation: The Journal of Chemical Physics **110**, 902 (1999); doi: 10.1063/1.478057
View online: http://dx.doi.org/10.1063/1.478057
View Table of Contents: http://scitation.aip.org/content/aip/journal/jcp/110/2?ver=pdfcov
Published by the AIP Publishing

JOURNAL OF CHEMICAL PHYSICS VOLUME 110, NUMBER 2 8 JANUARY 1999

Regular and irregular vibrational states: Localized anharmonic modes in Ar_3

Nicholas J. Wright and Jeremy M. Hutson[a]
Department of Chemistry, University of Durham, South Road, Durham, DH1 3LE, England

(Received 13 August 1998; accepted 9 October 1998)

We present a method for calculating the energy levels and wave functions of floppy triatomic molecules such as the rare gas trimers. It is based upon a potential-optimized discrete variable representation and takes into account the wide-amplitude vibrations that occur in such systems. We have investigated the energy levels and wave functions for Ar_3. The wave functions for the low-lying states show very regular behavior. Above the barrier to linearity, most of the wave functions are irregular but some have simple nodal patterns that suggest localization along periodic orbits. In addition to the ''horseshoe'' states previously described for H_3^+, we have identified localized features corresponding to symmetric and antisymmetric stretching vibrations around a linear configuration. The different localized modes can be combined to form more complex states in a manner analogous to normal modes. © *1999 American Institute of Physics.*
[S0021-9606(99)01402-6]

I. INTRODUCTION

The high-resolution spectra of Van der Waals trimers contain detailed information on the potential energy surfaces involved. Since the corresponding pair potentials are often very well known, the trimer spectra can in favorable cases be used to extract information on nonadditive intermolecular forces.[1–5] However, for this to be possible, precise and efficient methods of calculating the spectroscopic properties of trimers from potential energy surfaces are needed.

Bound-state calculations on Van der Waals trimers are challenging because the potential energy surfaces are strongly anharmonic, with low barriers to isomerization. The molecules often perform large-amplitude coupled motions, sampling a significant amount of configuration space. To make such problems computationally tractable, methods based upon the discrete variable representation (DVR) have often been used. The most extensive calculations to date have been performed on the H_3^+ molecular ion.[6–8] In this work we choose to concentrate instead on Ar_3 because we hope later to extend the methodology to Ar_2HF and Ar_2HCl, which are five-dimensional systems for which Ar_3 provides a prototype. In addition, the comparison between Ar_3 and H_3^+ should reveal how the dynamics depend on the potential energy surfaces and masses involved. Both Ar_3 and H_3^+ have equilibrium geometries that are equilateral triangles and both are very ''floppy,'' sampling large portions of the space of possible nuclear configurations. In both systems isomerization can occur via a linear transition state and the barrier is only about one third of the well depth.

The wave functions and energy level distribution of a polyatomic molecule reflect the underlying structure of its phase space. The high-lying vibrational states of such a system might be expected to be irregular because of the chaotic nature of the phase space at high energies. It is often found however that some states in this region have wave functions that are more localized; they show regular nodal patterns and do not sample all the energetically accessible phase space. In their studies of the high-lying vibrational states of H_3^+,[9–14] LiCN,[15] and KCN,[16] Tennyson and co-workers identified several types of localization effect. One of the aims of this work is to see whether the wave functions of Ar_3 show similar features, despite the different energy scales and masses involved.

There have been several previous calculations of the bound states of Ar_3. Horn *et al.*[17] used vibrational self-consistent-field theory in hyperspherical coordinates, while Leitner, Berry, and Whitnell[18] performed a DVR calculation in hyperspherical coordinates. Cooper, Jain, and Hutson[19] compared a variety of methods based on the normal mode, Jacobi, and hyperspherical coordinate systems. However, none of these calculations provide a reliable benchmark for the present work, either because of a lack computer power available at the time or because of programming errors as described in Ref. 19.

II. THEORY

A. Discrete variable representation

The theory of the discrete variable representation (DVR) method has been reviewed by Bačić and Light.[20] The DVR can be considered as representing the wave function in a basis set of spatially localized ''DVR functions,'' obtained by transformation of a corresponding set of spatially delocalized basis functions. The spatial localization is computationally advantageous, because it allows the DVR functions to be tailored to the regions of configuration space accessible for a particular system. Light *et al.*[21] show how to obtain a DVR for a particular coordinate by transforming the appropriate finite basis representation (FBR) Hamiltonian matrix ele-

---

[a] Electronic mail: j.m.hutson@durham.ac.uk

ments. In the case that the finite basis is a set of orthogonal functions, the DVR quadrature points and DVR-to-FBR transformation matrix can be obtained using the method of Harris, Engerholm, and Gwinn (HEG).[22]

A major advantage of the DVR method is that the matrix of the potential energy operator, $\hat{V}$, is taken to be diagonal, so that no multidimensional integrals over basis functions are required. Another advantage arises from the structure of the DVR Hamiltonian matrix, which can be exploited in the diagonalization procedure. The sparsity of the matrix makes it efficient to use an iterative eigenvalue solver,[7] while the fact that it is nearly block diagonal facilitates the use of sequential diagonalization and truncation (SDT) contraction schemes.[23,9] Iterative diagonalization and SDT contraction can be combined to good effect when using a parallel supercomputer.[24,25]

In the present work we use a Jacobi coordinate system to represent the ABC system as an atom A interacting with a diatom BC. The vector **r** of length r runs from atom B to atom C (where atom B is the heavier of B and C if they are different). The vector **R** of length R runs from the center of mass of BC to atom A. θ is the angle between **r** and **R**.

In this coordinate system the DVR Hamiltonian matrix elements are:

$$\begin{aligned}\mathbf{H}_{\alpha\beta\gamma K}^{\alpha'\beta'\gamma'K'} &= \sum_{ii'jj'll'} {}^{R}T_{i'\alpha'}\,{}^{r}T_{j'\beta'}\,{}^{K\theta}T_{l'\gamma'}H_{ijlK}^{i'j'l'K'}\,{}^{R}T_{i\alpha}\,{}^{r}T_{j\beta}\,{}^{K\theta}T_{l\gamma}\\ &= {}^{R}d_{\alpha'\alpha}\delta_{\beta'\beta}\delta_{\gamma\gamma'}\delta_{K'K}+{}^{r}d_{\beta'\beta}\delta_{\alpha'\alpha}\delta_{\gamma\gamma'}\delta_{K'K}+\frac{\hbar^2}{2}\left(\frac{1}{\mu_1R_\alpha^2}+\frac{1}{\mu_2r_\beta^2}\right){}^{\theta K}d_{\gamma'\gamma}\delta_{\alpha'\alpha}\delta_{\beta\beta'}\delta_{K'K}\\ &\quad+\frac{\hbar^2}{2\mu_1R_\alpha^2}\big([J(J+1)-2K^2]\delta_{\alpha'\alpha}\delta_{\beta'\beta}\delta_{\gamma\gamma'}\delta_{K'K}-[1+\delta_{K0}]^{1/2}\Lambda_{JK}^{+}B_{\gamma\gamma'K}^{+}\delta_{\alpha'\alpha}\delta_{\beta'\beta}\delta_{K'K+1}\\ &\quad-[1+\delta_{K'0}]^{1/2}\Lambda_{JK}^{-}B_{\gamma\gamma'K}^{-}\delta_{\alpha'\alpha}\delta_{\beta'\beta}\delta_{K'K-1}\big)+V_{\alpha\beta\gamma}^{\alpha'\beta'\gamma'}\delta_{K'K},\end{aligned} \tag{1}$$

where the notation of Choi and Light[26] is used. The first two terms are the kinetic energy operators associated with the two radial coordinates, R and r, the third term is the angular kinetic energy, the fourth term contains the centrifugal term and the Coriolis coupling, and the final term is the potential energy. The transformation matrices T are labeled by superscripts R, r, and $K\theta$ to indicate the coordinate that they refer to. Greek suffixes refer to DVR points and Roman suffixes to FBR functions. The reduced masses μ_1 and μ_2 correspond to the complete complex ($2M_{\mathrm{Ar}}/3$ here) and the diatom ($M_{\mathrm{Ar}}/2$ here), respectively. All calculations in the present work are for $J=0$, so that the centrifugal term and the Coriolis coupling are zero, but our implementation allows for $J\neq 0$.

B. Basis functions

The nth wave function of the system, with parity p and total angular momentum J, may be expanded in a finite basis representation as

$$\Psi_n^{pJ}(R,r,\theta)=R^{-1}r^{-1}\sum_{ijlK} c_{ijlKn}^{Jp}\,\phi_i^R(R)\,\phi_j^r(r)P_l^K(\cos\theta), \tag{2}$$

where the functions $P_l^K(\cos\theta)$ are associated Legendre polynomials. The functions $\phi_i^R(R)$ and $\phi_j^r(r)$ are potential-optimized basis functions in R and r (described below).

To generate the potential-optimized functions $\phi_i^R(R)$ for the R coordinate, solutions of a one-dimensional reference Hamiltonian, ${}^{1D}\hat{H}_{\mathrm{ref}}^R$, are calculated numerically using the `SCHRQ`[27] subroutine. In the present work, ${}^{1D}\hat{H}_{\mathrm{ref}}^R$ is taken to be

$${}^{1D}\hat{H}_{\mathrm{ref}}^R=-\frac{\hbar^2}{2\mu_1}\frac{\partial^2}{\partial R^2}+V_b^R(R), \tag{3}$$

where

$$V_b^R(R)=\frac{\hbar^2}{2\mu_1}\frac{L_m(L_m+1)}{R^2}+V_{\mathrm{min}}^R(R) \tag{4}$$

and $V_{\mathrm{min}}^R(R)$ is obtained by minimizing $V(R,r,\theta)$ with respect to r at $\theta=90°$ (see Fig. 1).

The definition of $V_b^R(R)$ in Eq. (4) includes L_m, which is the minimum value of L (the quantum number corresponding to end-over-end rotation in a space-fixed representation) for each symmetry block. The symmetry blocks are explained in more detail below, but for now we note that in the even (A_1/E) symmetry block L is always even and therefore L_m is 0. For the odd (A_2/E) block L is always odd and L_m is 1. This term prevents any DVR points for the odd symmetry block being placed in the unsampled region of space near $R=0$, where they would be redundant (and cause numerical problems).

The procedure used to define the basis functions $\phi_j^r(r)$ for the r coordinate is similar except that $V_{\mathrm{min}}^r(r)$ is obtained by minimizing $V(R,r,\theta)$ with respect to R, at both $\theta=90°$ and $0°$, and taking the lower of the two results. No $L_m(L_m+1)$ term is included here because the limit $r=0$ corresponds to nuclear coalescence and is excluded by $V(R,r,\theta)$.

TABLE I. A sample of the energy levels calculated for Ar_3. The potential minimum is at $-298.65\ cm^{-1}$. The full list is available electronically (Ref. 34).

	A_1/E		A_2/E	
Γ	n	E_n (cm^{-1})	E_n (cm^{-1})	n
A_1	1	-254.89		
E	2	-232.38	-232.38	1
A_1	3	-224.29		
A_1	4	-211.95		
E	5	-211.83	-211.83	2
...	...	...	...	...
A_1	17	-173.52		
E	18	-173.43	-173.43	10
A_1	19	-172.75		
E	20	-172.42	-172.42	11
E	21	-171.79	-171.79	12
A_1	22	-171.61		
A_2			-171.21	13
...	...	...	...	...
E	56	-145.85	-145.85	35
A_2			-145.82	36
A_1	57	-145.37		
E	58	-144.64	-144.64	37
A_1	59	-144.12		
E	60	-144.07	-144.07	38
...	...	...	...	...
E	285	-89.48	-89.48	235
A_1	286	-89.27		
E	287	-89.25	-89.23	236
A_1	288	-89.14		
E	289	-89.07	-89.07	237
A_2			-89.05	238
E	290	-88.99	-89.01	239
A_1	291	-88.95		

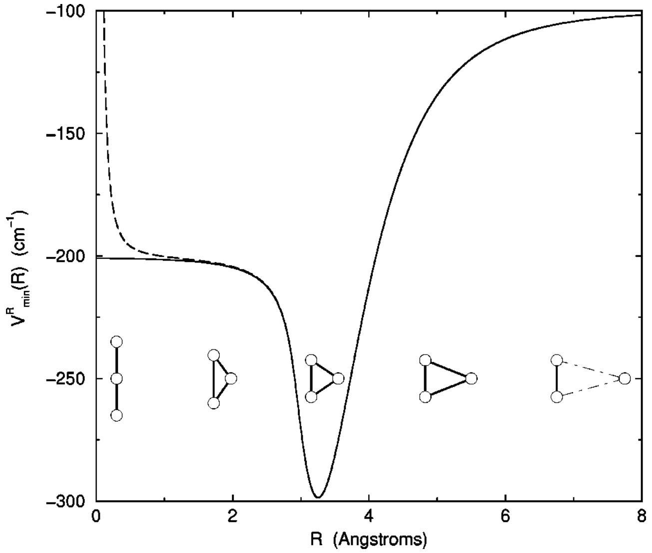

FIG. 1. The one-dimensional potential energy function used to obtain the potential-optimized DVR quadrature points in R. The dashed line shows the potential including the centrifugal term that is used for the odd symmetry block. The atomic configurations at selected points are shown to illustrate the isomerization pathway.

The basis-generating potentials $V_b^R(R)$ and $V_b^r(r)$ are designed to ensure that the basis sets span all values of one coordinate that are accessible at any value of another. The numerical functions obtained by solving the corresponding one-dimensional Hamiltonians are used in a calculation based on the HEG[22] method to obtain potential-optimized DVR (PO-DVR)[28] points in the required range.

C. Symmetry

The molecular symmetry group of Ar_3 is $D_{3h}(M)$. However, the only symmetry operation that appears naturally in Jacobi coordinates is permutation of the labels of the 'diatom' nuclei, which has the effect $\theta \rightarrow \pi - \theta$. Use of the Jacobi coordinate system effectively reduces the molecular symmetry group to $C_{2v}(M)$. The Hamiltonian matrix splits into two blocks, symmetric and antisymmetric with respect to the permutation. In terms of labels of $D_{3h}(M)$, the even block contains A_1 and E (component 1) and the odd block contains A_2 and E (component 2). The symmetric block contains only functions with l even in Eq. (2) and the odd block contains only functions with l odd.

Since the linear geometry with $R=0$ is accessible in Ar_3, some care is needed to establish the boundary conditions that apply there.[29,7,8] Since $\Psi(R,r,\theta)$ must be finite or zero at $R=0$, the basis functions $\phi_i^R(R)$ must be zero at the origin because of the R^{-1} factor in Eq. (2). It is possible to generate such functions that are either even or odd with respect to the transformation "$R \rightarrow -R$"[8] (though the concept of $R<0$ is not meaningful for Jacobi coordinates as defined here). Mandelshtam and Taylor[8] found empirically that odd parity functions give the best convergence for the even (A_1/E) symmetry block and even parity functions give the best convergence for the odd (A_2/E) symmetry block.

The pairings may be explained as follows. In the even symmetry block, $\Psi(R,r,\theta)$ is finite at $R=0$. To achieve this, $\lim_{R\rightarrow 0} R^{-1}\phi_i^R(R)$ must be finite, so that $\phi_i^R(R)$ itself must be linear in R near the origin. This is achieved by generating basis functions $\phi_i^R(R)$ with a node at $R=0$ but a finite derivative. These correspond to functions that are odd with respect to the transformation "$R \rightarrow -R$." Conversely, in the

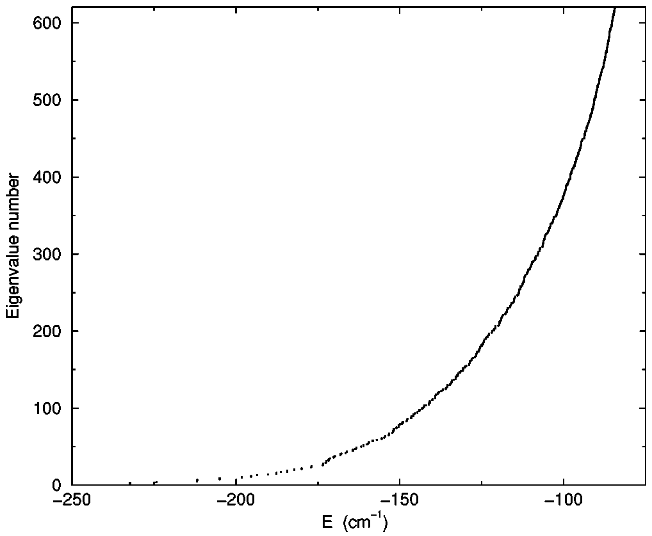

FIG. 2. The eigenvalue distribution of Ar_3. The density of states is the gradient of the curve. The increase in the density of states above the barrier to linearity is clearly visible around $-170\ cm^{-1}$.

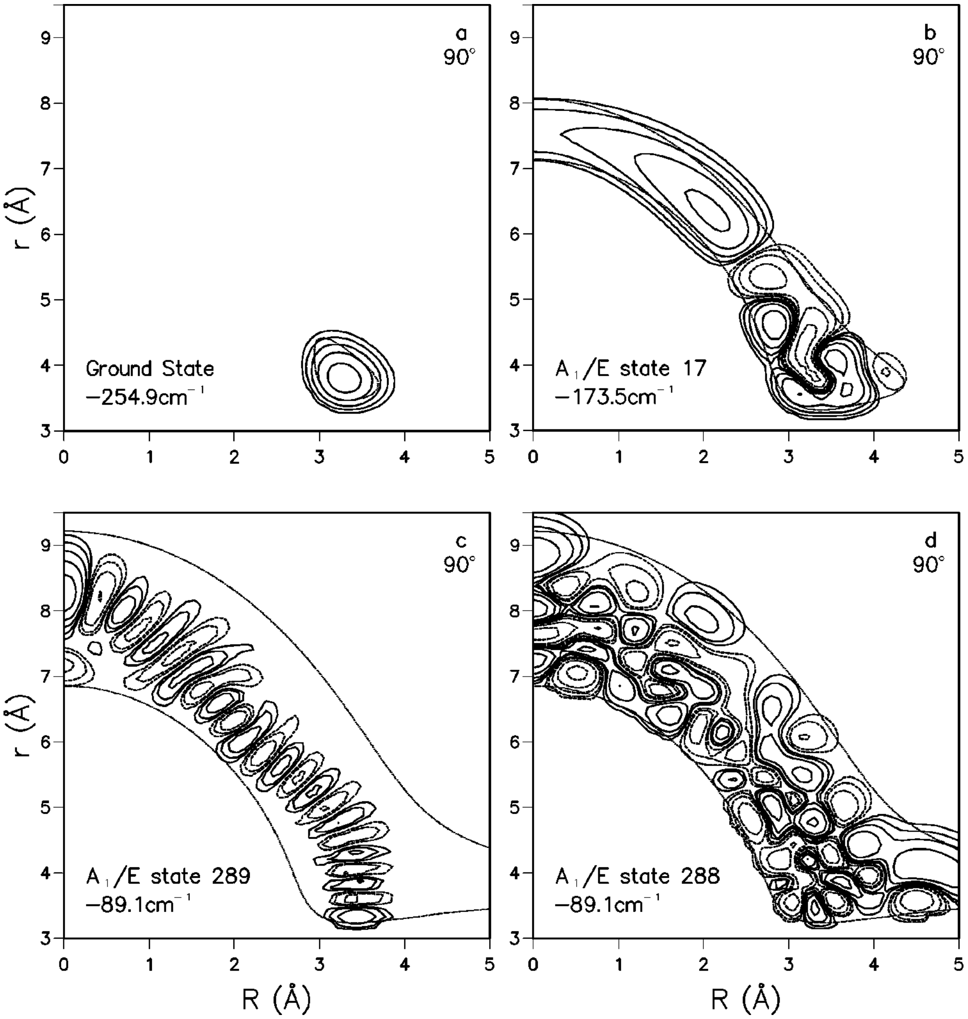

FIG. 3. Wave functions of Ar_3 plotted in Jacobi coordinates as a function of R and r for $\theta = 90°$. The dotted line shows the boundary of the classically allowed region of configuration space at the energy concerned. Solid and dashed contours show positive and negative values of the wave function, respectively. Contours are for 0.64, 0.32, 0.16, 0.08, and 0.04 of the maximum amplitude.

antisymmetric block, $\Psi(R,r,\theta)$ is zero at $R=0$. To achieve this, $\lim_{R\to 0} R^{-1}\phi_i(R)$ must be zero, so that $\phi_i^R(R)$ itself must have a zero value *and derivative* at the origin. The simplest such functions are those that are quadratic in R near the origin, which are even with respect to the transformation $R\to -R$.

D. Lanczos diagonalization

We obtain the eigenvalues and eigenvectors of the Hamiltonian matrix using the implicitly restarted Lanczos method (IRLM) as outlined by Sorensen.[30,31] The method does not require explicit construction of the Hamiltonian matrix; only matrix-vector products involving the Hamiltonian are needed. This allows diagonalization of matrices far larger than could be stored in computer memory. The computational cost of the IRLM can be broken down into two pieces. The first is associated with the internal numerical operation over the IRLM routines, over which the user has little control. The second is associated with the calculation of the matrix-vector products, which can be made very efficient because of the sparsity of the DVR Hamiltonian matrix.

The rate of convergence of the IRLM towards a solution depends on the eigenvalue distribution of the Hamiltonian matrix. The rate of convergence is inversely proportional to the difference between the the largest and smallest eigenvalues (the range of the spectrum.) The IRLM also converges best if the eigenvalues of interest are well separated from the rest of the spectrum. To improve the separation of the eigenvalue spectrum, we use the Chebychev polynomial preconditioning scheme described by Korambath, Wu, and Hayes.[32] This involves finding the eigenvectors of a polynomial function of the matrix and then using them to obtain the eigenvalues of the original matrix.

When constructing a DVR grid in the R coordinate, special attention must be paid to the behavior near the origin, $R=0$, which corresponds to one atom lying exactly midway between the other two (a linear geometry). For Ar_3 the barrier to linearity is relatively low, so that this region must be modeled carefully if states above the barrier are to be accurate. The angular kinetic energy involves a factor of R^{-2}, and is thus singular at $R=0$ unless $L=0$. As long as no DVR quadrature point is placed exactly at $R=0$, this does not introduce an actual singularity into the DVR Hamiltonian matrix. Nevertheless, close to $R=0$ it is not adequate to assume that the R^{-2} operator is diagonal in the DVR representation. In their calculation on H_3^+, Henderson, Tennyson, and Sutcliffe[6] found that assuming the R^{-2} operator was diagonal produced nonvariational convergence of the energy levels. Correction for the effect is simple using our numerical potential-optimized functions, because the matrix of the

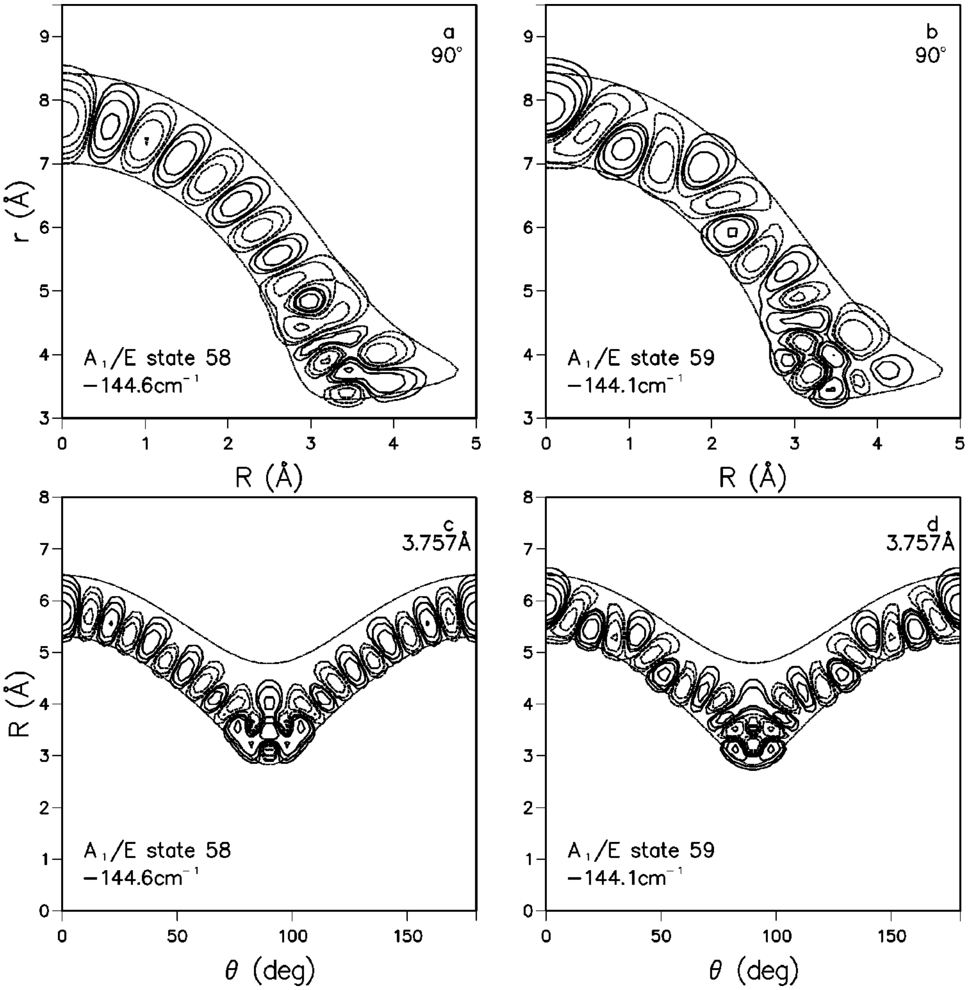

FIG. 4. Wave functions of Ar_3 plotted as in Fig. 3 and as a function of r and θ for $r=3.757$ Å. The dotted line shows the boundary of the classically allowed region of configuration space at the energy concerned. Solid and dashed contours show positive and negative values of the wave function, respectively. Contours are for 0.64, 0.32, 0.16, 0.08, and 0.04 of the maximum amplitude.

$1/R^2$ operator in the FBR can be computed accurately by numerical quadrature (Simpson's rule) and then transformed into the DVR. This gives angular kinetic energy terms that are off-diagonal between different points in R, which makes computation of the product of the Hamiltonian and the trial vector in the Lanczos diagonalization a little more expensive, but not prohibitively so.

The large matrix elements of R^{-2} term also lead to a large spectral range for the Hamiltonian matrix, which inhibits its efficient diagonalization. One way of dealing with this is that used by Mandelshtam and Taylor,[8] who defined an upper limit for the matrix elements of the angular kinetic energy operator; any matrix element above this limit was set equal to it. This approach, although successful in their work, does not mix well with the correction for the failure of the DVR quadrature approximation described above. The truncation must be done before transforming to the DVR, and this destroys the separability of the angular kinetic energy operator. Successive diagonalization and truncation provides a more elegant way to remove the unphysically large components of the angular kinetic energy matrix; in our implementation, we first diagonalize a (relatively small) DVR matrix evaluated at fixed r (with basis functions for R and θ) and then reject eigenvectors corresponding to large eigenvalues in choosing the basis set for the final Lanczos diagonalization.

E. Potential energy surface

The potential energy surface for a trimer, ABC, may be decomposed into pairwise-additive and nonadditive contributions,

$$V_{\mathrm{trimer}}=V_{\mathrm{AB}}(r_{\mathrm{AB}})+V_{\mathrm{BC}}(r_{\mathrm{BC}})+V_{\mathrm{AC}}(r_{\mathrm{AC}})+V_{\mathrm{nonadd}}, \quad (5)$$

where r_{AB}, r_{BC}, and r_{AC} are the interatomic distances. In the present work we have used the pairwise-additive approximation which neglects the relatively small term V_{nonadd}. In the present work, the zero of energy corresponds to infinitely separated atoms.

The potential energy surface for Ar_3 is constructed using the HFDID1 Ar–Ar pair potential of Aziz,[33] which has a well depth $\epsilon=99.55\ \mathrm{cm}^{-1}$ at an interatomic distance $r_m=3.757$ Å. The resulting Ar_3 surface has a well depth of $3\epsilon\approx 299\ \mathrm{cm}^{-1}$. Any pairwise-additive surface for an atomic trimer has a barrier to linearity that is very close to the pair potential well depth, about 100 cm^{-1} in this case. The lowest dissociation channel, to $Ar+Ar_2$ $(v=0)$ lies 85 cm^{-1} below the separated atoms, and thus 214 cm^{-1} above the equilibrium geometry.

III. RESULTS AND DISCUSSION

We have attempted to calculate the energy levels and wave functions for all $J=0$ bound states of Ar_3. The DVR basis set was constructed using 34 points in θ, 46 points in R, and 38 points in r. The 34 angular points with $\theta < 90°$ were taken from a 68-point Gauss-Legendre quadrature. The quadrature points in R were obtained by applying the HEG procedure to 46 numerical basis functions, which were in turn obtained by integrating the one-dimensional Schrödinger equation [Eq. (3)] from $R=0$ to 8 Å. The quadrature points in r were obtained similarly, propagating from $r=3$ to 10 Å. SDT contraction was not used in these calculations because of memory limitations, although it is implemented in our program.

Samples of the energy levels obtained in different energy regimes are given in Table I; the complete set is available electronically.[34] The large majority of the states lie above the barrier to linearity. We obtain 336 states from the even symmetry block $(N_{A_1}+N_E)$ and 277 states from the odd symmetry block $(N_{A_2}+N_E)$ below the lowest dissociation channel. It is likely that we have missed at least a few long-range levels very close to dissociation. The difference between the energies of corresponding E levels in the even and odd symmetry blocks provides a useful measure of the basis-set convergence and suggests that our results are accurate to about ± 0.05 cm^{-1}. However, the high density of states makes identification of E levels from near-degeneracies unreliable at high energies.

The cumulative energy level distribution is shown in Fig. 2; the density of states is the gradient of this. The density of states shows a sharp increase near the barrier to linearity, where a significant amount of extra phase space becomes accessible. The density then increases fairly steadily

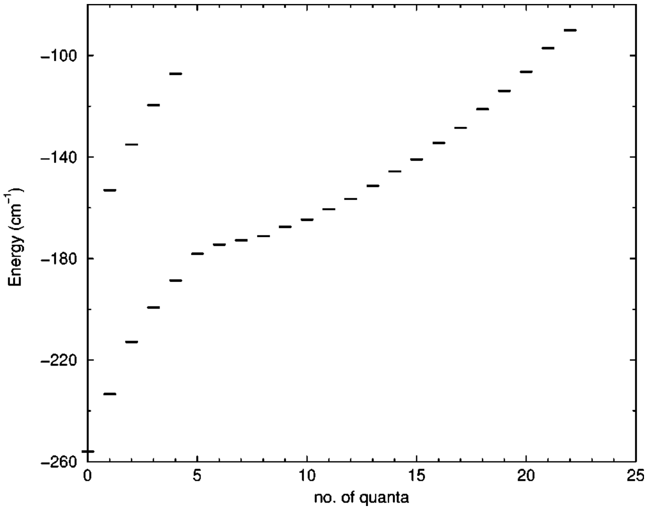

FIG. 5. Progression of regular states in Ar$_3$. The lower set of levels are the horseshoe-like states, and the upper set are the ''linear symmetric stretch'' levels.

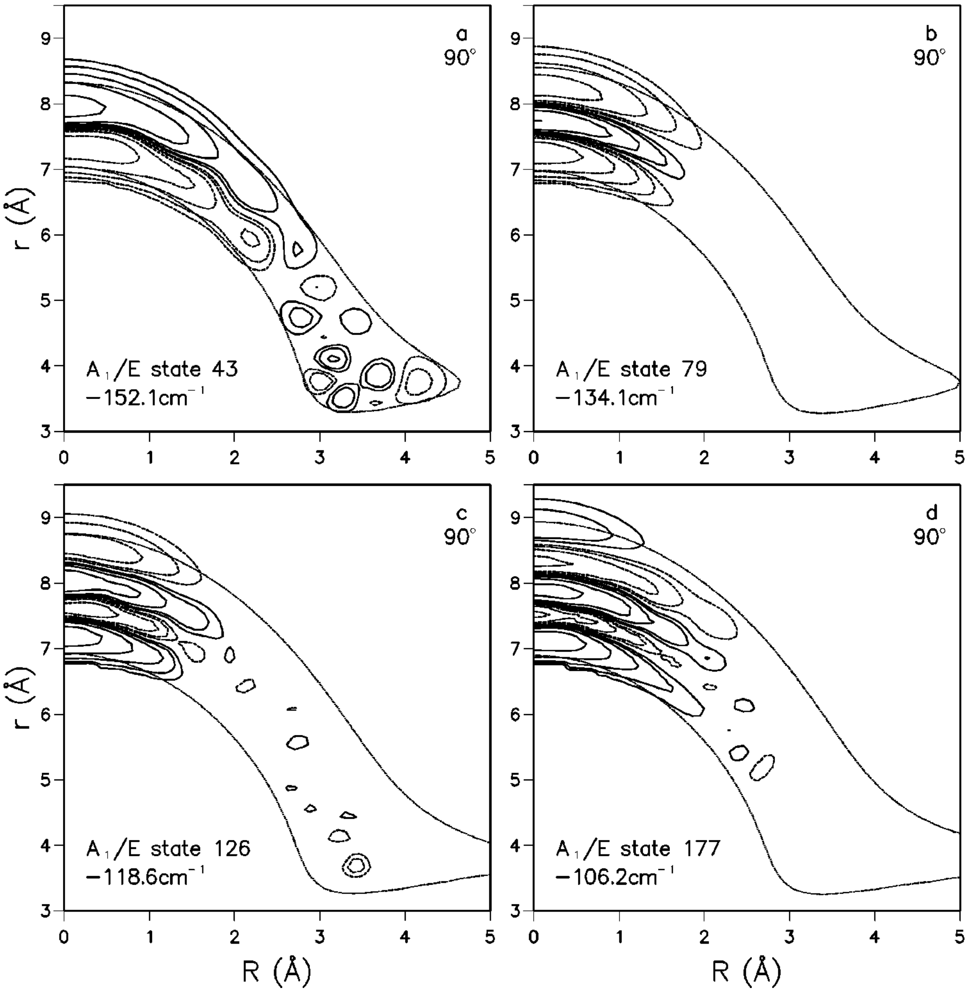

FIG. 6. Wave functions for states involving excitation in the linear symmetric stretch mode, plotted as in Fig. 3. (a)–(d) show states with $n_s=1$ to 4.

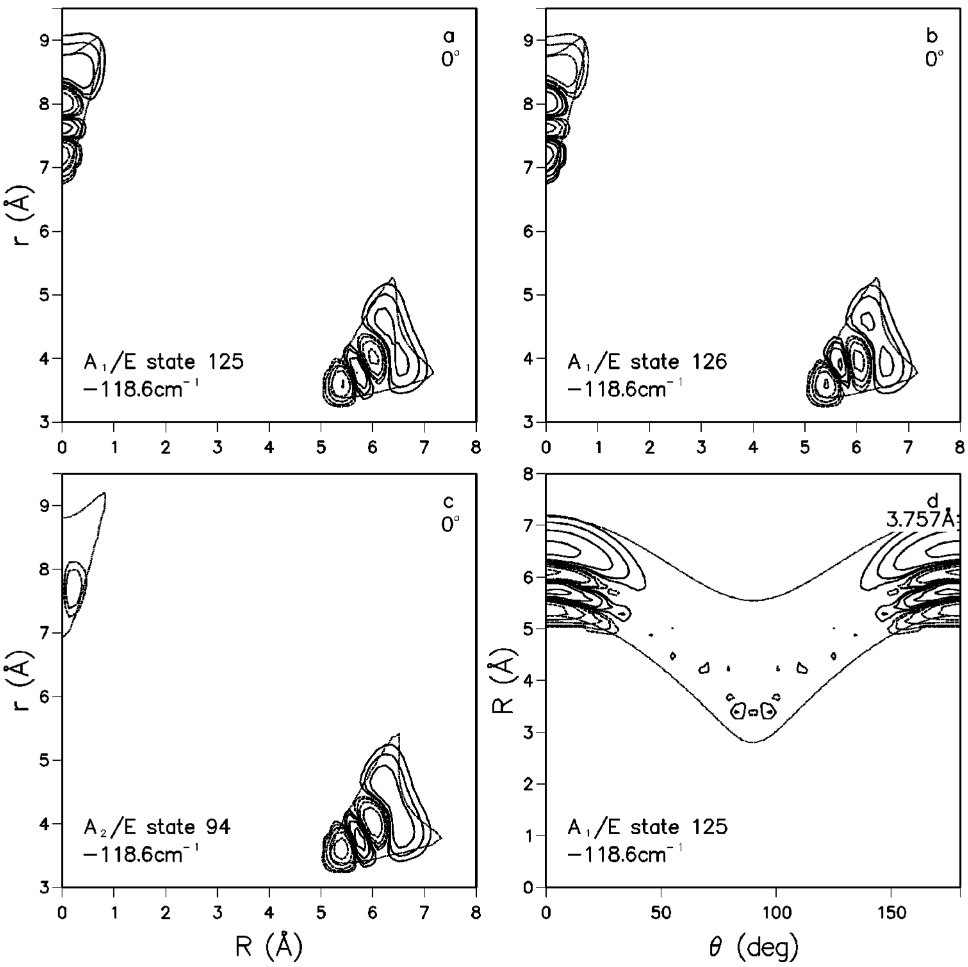

FIG. 7. Wave functions for states of different symmetry with $n_s=3$ in the linear symmetric stretch mode, plotted as in Fig. 4.

from about 2 states/cm^{-1} at the barrier maximum to about 8 states/cm^{-1} at $E=-100$ cm^{-1}.

It is interesting to compare the wave functions for Ar_3 with those for H_3^+.[9,11–14] Examples of the present results are shown as contour plots in Fig. 3. Since the wave functions are functions of three coordinates, they are presented here as cuts at either fixed θ or fixed r. Other representations can be envisaged, but these appear to be the most helpful for present purposes. The R^{-1} and r^{-1} factors in Eq. (2) have been included, because without them all the wave functions appear to have a nodal plane at $R=0$.

Normal mode quantum numbers are not appropriate for highly excited states of floppy molecules. For H_3^+, an assignment in terms of normal modes has been possible only up to the fourth polyad.[14] For Ar_3, there are only six vibrational levels that lie below the classical barrier to isomerization. The effective barrier is raised somewhat by zero-point energy at the transition state, but nevertheless only the lowest few levels can be assigned in terms of normal modes. For Ar_3 on the HFD-C potential energy surface,[35] Cooper, Jain, and Hutson,[19] were able to assign the first excitation in each mode and some of the states in the second polyad. The HF-DID1 potential[33] used in the present work is qualitatively similar, and the assignments of the low-energy states are the same.

The classical isomerization barrier occurs at -199 cm^{-1}. At the linear geometry, Ar_3 is expected to have about twice the zero-point energy of Ar_2 (15 cm^{-1}), so the first level to sample the region around linearity significantly is expected near -170 cm^{-1}. The first state that actually has significant amplitude around $R=0$ is the 17th state of A_1/E symmetry at -173.5 cm^{-1}. The wave function for this state is shown in Fig. 3(b), along with that for the ground state [Fig. 3(a)].

In H_3^+, extensive localization effects were observed in the wave functions of states lying above the barrier to linearity.[12–14] In particular, Tennyson and co-workers[12,13] observed a progression of ''horseshoe'' states, in which one H atom moves between the other two (and out the other side), with the two ''outer'' atoms moving apart to make way for it. The horseshoe states are so-called because their wave functions show a regular nodal pattern that follows a horseshoe-shaped curve in a representation such as Fig. 3, including the reflection to negative R. In H_3^+, the ''regular'' horseshoe states are embedded in a ''bath'' of irregular states, and in most cases the horseshoe character is spread over a considerable number of eigenstates. Under these circumstances, correlation functions[13] were found useful in analyzing the underlying regular features. The positions of the horseshoe states correspond to intensity peaks in the calculated spectrum.[12]

We have observed similar effects in Ar_3, as shown in Fig. 3. Once again there are a few regular states, with relatively simple nodal patterns, lying among and mixed with a dense bath of irregular states. A particularly clear example of a horseshoe state is shown in Fig. 3(c). The wave function may be contrasted with that for an irregular bath state such as that in Fig. 3(d). The wave function for the bath state shows no obvious nodal pattern and fills all the energetically available space.

A triatomic molecule can be described in terms of an atom A and a diatom BC in three different ways. Each Ar_3 geometry can thus be described by three different sets of Jacobi coordinates corresponding to different labelings of the atoms. For example, the symmetric linear geometry with $r_{\mathrm{AB}}=r_{\mathrm{BC}}=r_m$ can be described by $(R,r,\theta)=(0,2r_m,\text{undefined})$, $(1.5r_m,r_m,0°)$, and $(1.5r_m,r_m,180°)$. It is important to remember this when interpreting wave functions. This is illustrated in Fig. 4, which shows two neighboring states with horseshoe character. The wave functions are shown both as functions of R and r for $\theta=90°$ and as functions of R and θ for $r=r_m=3.757$ Å. Although the paths followed in coordinate space are quite different in Figs. 4(a) and 4(c), the molecular configurations involved are in fact the same: another way to view the horseshoe motion is as an Ar atom rotating around the end of an Ar_2 diatom.

One difference between Ar_3 and H_3^+ is that in Ar_3 there are fewer bath states underlying each regular state, and the regular character is generally spread over a few eigenstates at most. The regular patterns can be seen more easily in the wave functions for Ar_3 than for H_3^+. The progression of horseshoe-like states can be followed all the way down to the ground state, although below the barrier to linearity the horseshoe is ''broken,'' with no amplitude near $R=0$. The resulting energy level pattern is shown in Fig. 5, and shows a remarkably regular (though strongly anharmonic) progression, with a plateau that corresponds to the barrier to linearity.

We have observed several additional types of localization effect (''localized anharmonic modes'') in Ar_3. Most of these can be explained in terms of vibrations about a symmetrical linear geometry, which corresponds to a saddle point on the potential energy surfaces of both H_3^+ and Ar_3. Indeed, the horseshoe motion can be considered as a (very) wide-amplitude bending motion about such a geometry. Symmetric and antisymmetric stretching vibrations about the linear geometry can also be envisaged, and both these are observed in one form or another.

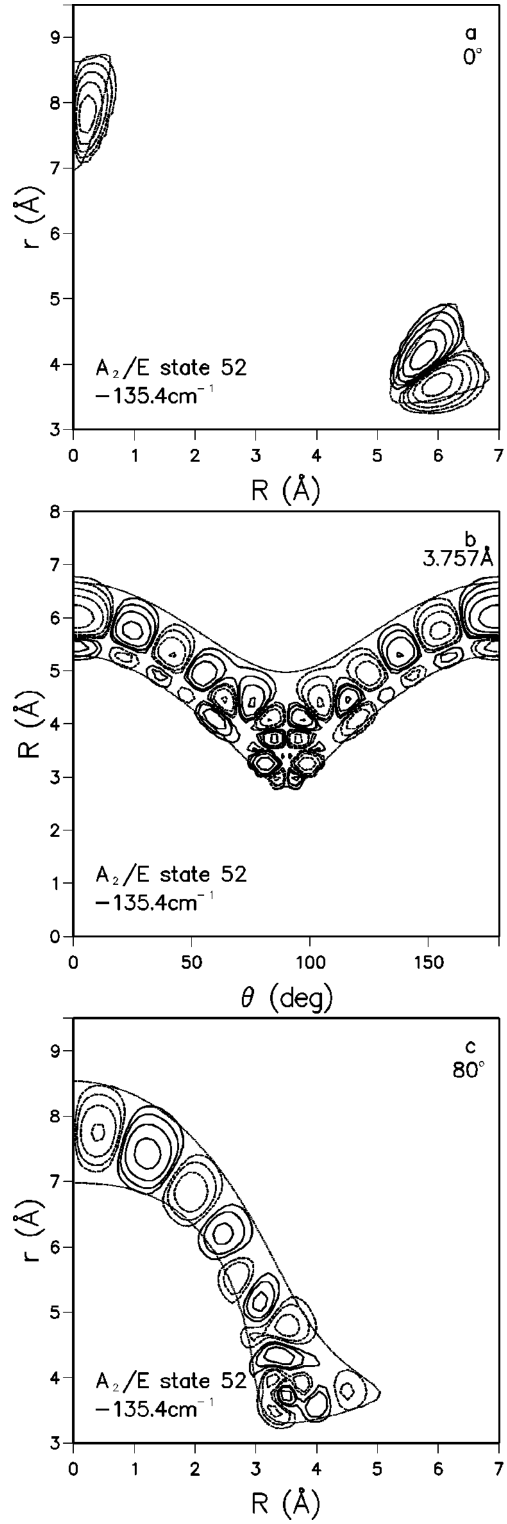

FIG. 8. Wave functions for states involving one quantum of excitation in the atom–diatom intermolecular stretch mode, plotted as in Fig. 4. This mode corresponds to the linear asymmetric stretch at $\theta=0$ and to the horseshoe mode near $\theta=90°$.

The linear symmetric stretch mode is most clearly seen as excitation in the r coordinate with R close to zero. Figure 6 shows states with quantum numbers $n_s=1$ to 4 in this mode. The symmetric stretch energy levels also show a regular progression, as shown in Fig. 5. The equilibrium geometry of Ar_2 has $r_m=3.757$ Å, so the three equivalent linear saddle point structures have $(R,r,\theta)\approx(0,\ 7.52\ \text{Å},\ \text{undefined})$, (5.64 Å, 3.76 Å, 0°) and (5.64 Å, 3.76 Å, 180°). The wave functions for the three states with $n_s=3$ are shown in Fig. 7, and may be seen to show amplitude at all three geometries. Note that the symmetric stretch corresponds to R and r increasing *in phase* with one another in the feature at $r=r_m$. The properly symmetrized states are combinations of the states localized about the three equivalent linear geometries, with A_1 and E symmetry in the molecular symmetry group $D_{3h}(M)$. It may be seen that our basis set (which does not explicitly impose this symmetry) has produced reasonably well-symmetrized wave functions for these three states. As expected, two of the states [A_1, Fig. 7(a), and one component of E, Fig. 7(b)] are in the even symmetry block, and the third is in the odd block. Figure 7(d) shows the A_1 state

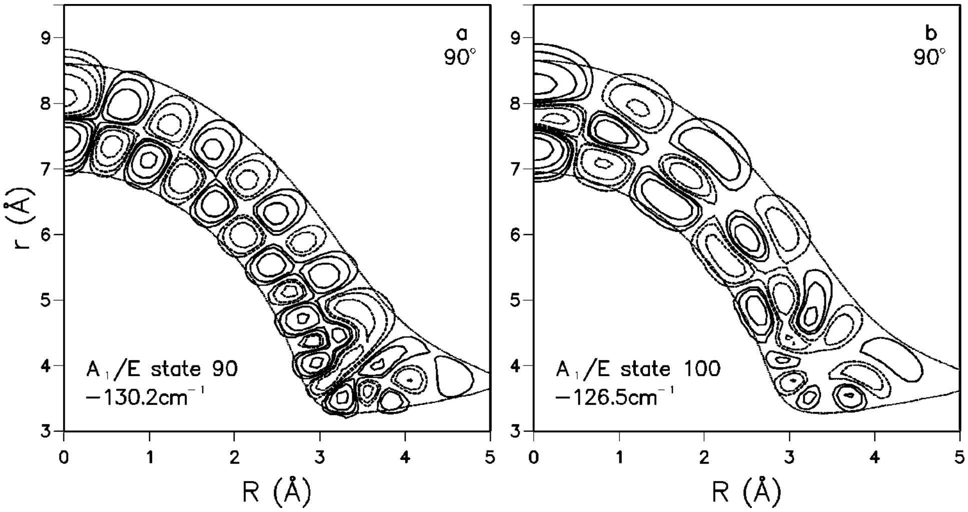

FIG. 9. Wave functions for states involving simultaneous excitation in the linear symmetric stretch and horseshoe modes, plotted as in Fig. 3.

for $n_s = 3$ as a function of R and θ for $r = r_m$; it may be seen that the function is indeed localized around the linear configuration(s), and does not undergo large angular excursions.

We also looked for the antisymmetric stretch mode. The obvious place to look for it is at $\theta = 0$, as excitations in R about $R = 0$ with $r \approx 2r_m$. Such features are indeed observed, as seen in Fig. 8(a) (which is for a state in the odd block, because a node is required at $R = 0$). This state also shows amplitude around the configuration corresponding to the ''reordered'' linear geometries. Since this is an antisymmetric stretch, R and r increase *out of phase* with one another in the feature at $r = r_m$. However, in this case the amplitude is *not* confined to the linear geometries. Figure 8(b) shows the wave function as a function of R and θ for $r = r_m$ and Fig. 8(c) shows it as a function of R and r for $\theta = 80°$ (because there is a node at $\theta = 90°$): the molecule is clearly undergoing horseshoe-type motion in addition to the antisymmetric stretch. The stretching motion involved here is perhaps best considered as the intermolecular stretch of an atom–diatom complex. At $\theta = 0$, the radial motion in Fig. 8(b) is essentially the asymmetric stretch of a linear molecule, but near $\theta = 90°$ the amplitude of the ''stretching'' motion is enough to carry the atom through the center of the diatom, and this is the horseshoe motion.

It is interesting that localized anharmonic modes can be combined in much the same way as normal modes. Figures 9(a) and 9(b) show another pair of localized states which are combinations of the symmetric stretch and horseshoe modes. These states are similar to the ''nodal horseshoe'' described for H_3^+ in Ref.36. The fact that the nodal horseshoe is a combination of two localized modes suggests that the linear symmetric stretch mode is probably present in H_3^+ as well.

In H_3^+, the regular states are localized along the trajectories of classical periodic orbits.[37] A study of the periodic orbits of Ar_3 on the potential energy surface used here has been carried out,[38] but it concentrated on Ar + Ar_2 collisions (at energies above those relevant to bound states). Calculating the bound-state periodic orbits of Ar_3 is beyond the scope of the present work, but it seems reasonable to attribute the localization effects observed here to such orbits. Investigating the connection between the localization effects and periodic orbits of Ar_3 would be an interesting topic for future work.

The picture of regular features spread over several states accords with the standard ''time-independent'' picture of intramolecular vibrational energy redistribution[39] (IVR): when a regular state is embedded in a dense bath of other states, the character of the regular state is spread out over the bath states, its contribution peaking as a function of energy in a near-Lorentzian manner. At higher energies, the density of bath states is greater and the ''regular'' character is spread over more energy levels. If the bath is dense enough, it may turn out that no one eigenstate ends up with a significant amount of regular character. Such effects can be thought of as the bound state analogue of quantum mechanical scattering resonances. When the quasicontinuum becomes an actual (dissociative) continuum, the regular character is spread out over the width of the resulting predissociating state.

IV. CONCLUSIONS

We have developed a method of calculating the energy levels and wave functions of floppy triatomic molecules based upon the potential-optimized discrete variable representation (PO-DVR). The method allows accurate calculations on states above the barrier to isomerization by the use of a numerical finite basis representation from which the corresponding PO-DVR is obtained.

Most of the states that lie above the isomerization barrier are irregular in character; they fill all the energetically accessible configuration space, and their wave functions have no obvious nodal pattern. However, embedded among these irregular states are some more regular states, which are more localized and have simple nodal patterns. The regular and irregular states are mixed to a greater or lesser extent, and in some cases the regular character is spread over several eigenstates. This general behavior is similar to that observed previously for the H_3^+ molecular ion.

The horseshoe localization effect previously observed in H_3^+ is also present in Ar_3. We have also found additional types of localization effect, corresponding to symmetric and antisymmetric stretching motions about a linear configuration. Even the horseshoe mode can be considered as the bending motion of a linear molecule. The different localized modes can be combined to form more complex localized features.

The wave functions of floppy molecules reveal a fascinating range of dynamical behavior. Future work in this area should lead to a better understanding of the relationship between the quantum and classical descriptions of such systems. At the moment it is possible to calculate the wave functions and explain their localized features with reference to the periodic orbits of the system. A theory in which the periodic orbits are used to predict the quantum behavior is, however, not yet available. By studying a range of different molecules, it may be possible to develop such a theory.

ACKNOWLEDGMENTS

We are grateful to Dr. Robert Bryan, Dr. Rita Prosmiti, and Professor Jonathan Tennyson for valuable discussions, and Professor Edward Hayes and Prakashan Korambath for sending us the routines for their implementation of the IRLM with polynomial preconditioning. N. J. W. thanks the EPSRC for a research studentship and Durham University Chemistry Department for a research scholarship. The calculations were carried out on a Silicon Graphics Origin 2000 computer system, which was purchased with funding from the EPSRC. We are grateful to Dr. Lydia Heck for her assistance in this context.

[1] A. R. Cooper and J. M. Hutson, J. Chem. Phys. **98**, 5337 (1993).
[2] M. J. Elrod and R. J. Saykally, Chem. Rev. **94**, 1975 (1994).
[3] A. Ernesti and J. M. Hutson, Phys. Rev. A **51**, 239 (1995).
[4] A. Ernesti and J. M. Hutson, J. Chem. Phys. **103**, 3386 (1995).
[5] A. Ernesti and J. M. Hutson, J. Chem. Phys. **106**, 6288 (1997).
[6] J. R. Henderson, J. Tennyson, and B. T. Sutcliffe, J. Chem. Phys. **98**, 7191 (1993).
[7] M. J. Bramley, J. W. Tromp, T. Carrington, Jr., and G. C. Corey, J. Chem. Phys. **100**, 6175 (1994).
[8] V. A. Mandelshtam and H. S. Taylor, J. Chem. Soc., Faraday Trans. **93**, 847 (1997).
[9] J. Tennyson and J. R. Henderson, J. Chem. Phys. **91**, 3815 (1989).
[10] O. Brass, J. Tennyson, and E. Pollak, J. Chem. Phys. **92**, 3377 (1990).
[11] J. R. Henderson and J. Tennyson, Chem. Phys. Lett. **173**, 133 (1990).
[12] C. R. Le Sueur, J. R. Henderson, and J. Tennyson, Chem. Phys. Lett. **206**, 429 (1993).
[13] G. Garćia de Polavieja, N. Fulton, and J. Tennyson, Mol. Phys. **83**, 361 (1994).
[14] D. A. Sadovski, N. G. Fulton, J. R. Henderson, J. Tennyson, and B. I. Zhilinskií, J. Chem. Phys. **99**, 906 (1993).
[15] J. R. Henderson and J. Tennyson, Mol. Phys. **69**, 639 (1990).
[16] J. R. Henderson, H. A. Lam, and J. Tennyson, J. Chem. Soc., Faraday Trans. **88**, 3287 (1992).
[17] T. R. Horn, R. B. Gerber, J. J. Valentini, and M. A. Ratner, J. Chem. Phys. **94**, 6728 (1991).
[18] D. M. Leitner, R. S. Berry, and R. M. Whitnell, J. Chem. Phys. **91**, 3470 (1989).
[19] A. R. Cooper, S. Jain, and J. M. Hutson, J. Chem. Phys. **98**, 2160 (1993).
[20] Z. Bačić and J. C. Light, Annu. Rev. Phys. Chem. **40**, 469 (1989).
[21] J. C. Light, I. P. Hamilton, and J. V. Lill, J. Chem. Phys. **82**, 1400 (1985).
[22] D. O. Harris, G. G. Engerholm, and W. D. Gwinn, J. Chem. Phys. **43**, 1515 (1965).
[23] Z. Bačić and J. C. Light, J. Chem. Phys. **85**, 4594 (1986).
[24] X. T. Wu and E. F. Hayes, J. Chem. Phys. **107**, 2705 (1997).
[25] H. Y. Mussa, J. Tennyson, C. J. Noble, and R. J. Allan, Comput. Phys. Commun. **108**, 29 (1998).
[26] S. E. Choi and J. C. Light, J. Chem. Phys. **92**, 2129 (1990).
[27] R. J. Le Roy, University Of Waterloo Chemical Physics Research Report **CP-555**, 1995.
[28] J. Echave and D. C. Clary, Chem. Phys. Lett. **190**, 225 (1992).
[29] J. Tennyson and B. T. Sutcliffe, J. Mol. Spectrosc. **101**, 71 (1983).
[30] D. C. Sorensen, SIAM J. Matrix Anal. Appl. **13**, 357 (1992).
[31] R. B. Lehoucq, K. Maschoff, D. C. Sorensen, and C. Yang, ARPACK, is available from `ftp://ftp.caam.rice.edu/pub/software/ARPACK`.
[32] P. P. Korambath, X. T. Wu, and E. F. Hayes, J. Phys. Chem. **100**, 6116 (1996).
[33] R. A. Aziz, J. Chem. Phys. **99**, 4518 (1993).
[34] The full list of energy levels are available via anonymous ftp from: `krypton.dur.ac.uk`.
[35] R. A. Aziz and H. H. Chen, J. Chem. Phys. **67**, 5719 (1977).
[36] G. Garćia de Polavieja, N. Fulton, and J. Tennyson, Mol. Phys. **87**, 651 (1996).
[37] J. Tennyson, O. Brass, and E. Pollak, J. Chem. Phys. **92**, 3005 (1990).
[38] K. M. Atkins and J. M. Hutson, J. Chem. Phys. **103**, 9218 (1995).
[39] M. Bixon and J. Jortner, J. Chem. Phys. **50**, 3284 (1969).